FULL PAPER

Dalton
www.rsc.org/dalton

The solution structure of homotrimetallic lanthanide helicates investigated with novel model-free multi-centre paramagnetic NMR methods †

Nadjet Ouali,[a] Jean-Pierre Rivera,[a] Pierre-Yves Morgantini,[b] Jacques Weber[b] and Claude Piguet*[a]

[a] *Department of Inorganic, Analytical and Applied Chemistry, University of Geneva, 30 quai E. Ansermet, CH-1211 Geneva 4, Switzerland. E-mail: Claude.Piguet@chiam.unige.ch*

[b] *Department of Physical Chemistry, University of Geneva, 30 quai E. Ansermet, CH-1211 Geneva 4, Switzerland*

Received 16th December 2002, Accepted 5th February 2003
First published as an Advance Article on the web 4th March 2003

The combination of one contact and three pseudo-contact contributions to the NMR hyperfine paramagnetic shift of each proton in the triple-stranded helicates $[Ln_3(L1)_3]^{9+}$ (Ln = Ce–Yb except Pm, Gd) produce intractable ^1H NMR spectra whose assignment is limited by the large electronic contribution to the nuclear relaxation processes. The detailed analysis of the NMR spectra for the diamagnetic complexes $[Ln_3(L1)_3]^{9+}$ (Ln = La, Lu, Y) shows that the triple-helical structure found in the solid state is maintained in solution. Extension of the classical one-nucleus crystal-field dependent model-free method for paramagnetic D_3-symmetrical homotrimetallic lanthanide complexes possessing two different metallic sites (*i.e.* two second-rank crystal-field parameters: $B_0^{2central}$ and $B_0^{2terminal}$) allows (i) the complete interpretation of the paramagnetic signals for Ln = Ce–Yb and (ii) the detection of a concomitant abrupt change of the contact terms F_i and of the pseudo-contact terms $S_i = B_0^{2central}G_i^1 + B_0^{2terminal}(G_i^2 + G_i^3)$ occurring near the middle of the lanthanide series. The derivation and application of a novel three-nuclei crystal-field independent method eventually demonstrates that the helicates $[Ln_3(L1)_3]^{9+}$ adopt a single D_3-symmetrical structure along the complete lanthanide series in solution, which ascribes the discontinuity observed for S_i to a concomitant decrease of the two crystal-field parameters. Comparison with structural models is limited by the extreme sensitivity of the structural factors C_{ikl} and D_{ikl} to minor geometrical variations affecting the wrapping of the ligand strands, but calculations of the geometrical factors G_i^m (m = 1–3) for $[Ln_3(L1)_3]^{9+}$ in solution confirm the formation of a regular triple-helical structure. Generalization of this novel three-nuclei method for addressing the solution structure of rhombic lanthanide complexes is discussed.

Introduction

Although the trivalent lanthanide metal ions (Ln^{III}) display variable and poorly controlled coordination spheres which limit structural programming, the global invariance of the electronic properties when going from the free ions to the complexes is attractive for designing specific functions in sophisticated supramolecular architectures.[1] For instance, the long-lived line-like visible emission of Eu^{III} and Tb^{III} has been systematically exploited for the development of sensitive heterogeneous[2] and homogeneous[3] fluoroimmunoassays, while the slow electronic relaxation of Gd^{III} ($4f^7$) has been extensively used for the design of MRI contrast agents in biological media.[4] On the other hand, an ultrafine tuning of the metal-centred electronic levels results from weak crystal-field effects induced by the surrounding donor atoms of the ligands and new properties can be induced in the lanthanide complexes which have no counterpart in the free ions.[5] In this context, large and tuneable paramagnetic anisotropies result from the removal of the spherical symmetry around Ln^{III} in coordination complexes,[6] thus producing considerable pseudo-contact contributions (δ_{ij}^{pc}) to the NMR shifts for a magnetically active nucleus i located in the vicinity of the paramagnetic centre j (eqn. (1), $\chi_{\alpha\alpha}^j$ are the components of the magnetic tensor in the principal magnetic axes system with Ln^{III} located at the origin, $\chi_{zz}^j - \frac{1}{3}Tr\chi^j$ and $\chi_{xx}^j - \chi_{yy}^j$ are respectively the axial and rhombic anisotropies, θ_i, ϕ_i and r_i are the internal polar coordinates and N_A is Avogadro's number).[7]

$$\delta_{ij}^{pc} = \frac{1}{2N_A}\left[\left(\chi_{zz}^j - \frac{1}{3}Tr\chi^j\right)\left(\frac{3\cos^2\theta_i - 1}{r_i^3}\right) + \left(\chi_{xx}^j - \chi_{yy}^j\right)\left(\frac{\sin^2\theta_i \cos 2\phi_i}{r_i^3}\right)\right] \quad (1)$$

For more than three decades, paramagnetic shift reagents have taken advantage of the pseudo-contact shifts for increasing the separation between closely-spaced signals in the NMR spectra,[8] but the systematic introduction of superconducting magnets now limits the interest for these devices. However, the recent design of new MRI-CEST contrast agents based on magnetization transfer for medical tomography,[9] and the tentative elucidation of the solution structures of sophisticated lanthanide complexes[10] are new challenges for rationally manipulating magnetic anisotropies and pseudo-contact shifts by using a simple approach accessible to co-ordination and supramolecular chemists.[11] In two seminal papers,[12] Bleaney proposed an expansion of the magnetic susceptibility tensor in a power series in the inverse of the temperature (T^{-n}) limited to $n \leq 2$ if $kT > \Delta E_{CF}$ (high-temperature expansion, ΔE_{CF} being the crystal-field splitting). While the T^{-1} term corresponds to the isotropic part of the tensor ($\frac{1}{3}Tr\chi^j$), the T^{-2} term describes

† Electronic supplementary information (ESI) available: tables of structural factors C_{ikl}, D_{ikl} obtained for the model complexes and for $[Ln_3(L1)_3]^{9+}$ in solution (Table S1) and geometrical factors calculated for the structure of $[Eu_3(L1)_3]^{9+}$ optimized in the gas phase (Table S2). Figures showing a plot of $1/T_{1i}^{para}$ *vs.* $\sum_{m=1}^{3}\frac{1}{\left(r_i^m\right)^6}$ according to eqn. (19) (Fig. S1), a plot of AF_{ikl} for the 165 H*ikl* triplets in $[Ln_3(L1)_3]^{9+}$ (Fig. S2) and comparisons of structural parameters between the optimized gas phase model and the solution structure (Figs. S3 and S4). See http://www.rsc.org/suppdata/dt/b2/b212352e/

DOI: 10.1039/b212352e

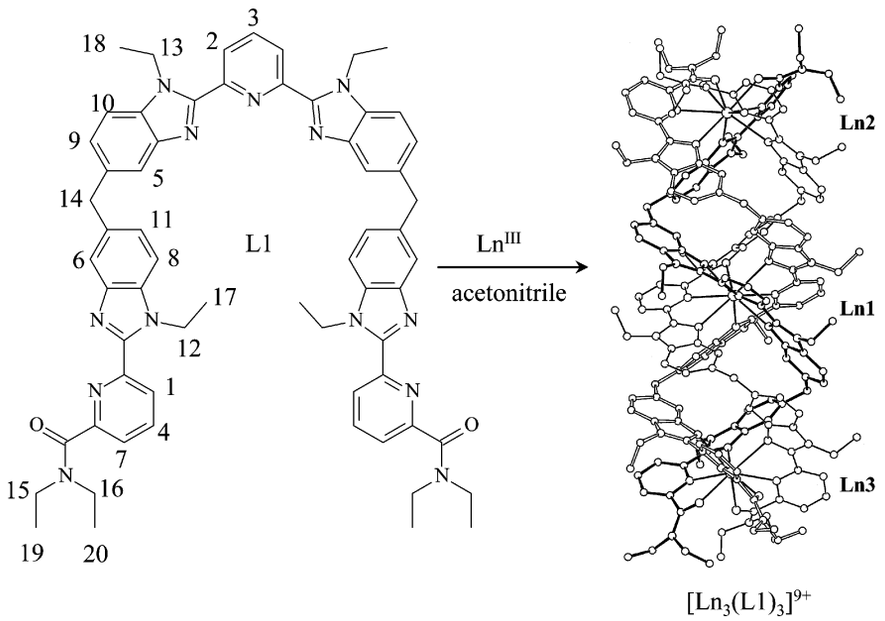

Fig. 1 Self-assembly of the D_3-symmetrical homotrimetallic helicates $[Ln_3(L1)_3]^{9+}$ in acetonitrile with numbering scheme. The representation of the complex corresponds to the crystal structure of $[Eu_3(L1)_3](CF_3SO_3)_9(CH_3CN)_9(H_2O)_2$.[16]

the anisotropic part of the tensor and provides a simple correlation between the paramagnetic anisotropies and the second-rank crystal-field parameters B_q^2 (eqn. (2) holds for the axial paramagnetic anisotropy and eqn. (3) for the rhombic paramagnetic anisotropy).[6,11,12]

$$\chi_{zz}^j - \frac{1}{3}Tr\chi^j = -\frac{\beta^2\left(1+p^j\right)\xi^j N_A}{60\left(kT\right)^2}B_0^2 \qquad (2)$$

$$\chi_{xx}^j - \chi_{yy}^j = -\frac{\beta^2\left(1+p^j\right)\xi^j N_A}{60\left(kT\right)^2}\sqrt{6}B_2^2 \qquad (3)$$

Substituting eqns. (2) and (3) into eqn. (1) gives the classical eqn. (4).[11] The first numerical terms $C_j = -\frac{\beta^2\left(1+p^j\right)\xi^j}{120\left(kT\right)^2}$, often referred to as Bleaney's factors, only depend on the electronic $4f^n$ configurations (*via* ξ^j and $(1 + p^j)$ which are numerical factors calculated for each $4f^n$ configuration),[6,11,12] and their relative values (scaled to $C_{Dy} = -100$) have been tabulated at 300 K.[10–13] $G_i = (3\cos^2\theta_i - 1)/r_i^3$ and $H_i = (\sin^2\theta_i \cdot \cos 2\phi_i)/r_i^3$ are the geometrical terms which contain the structural information required for solving the solution structure of lanthanide complexes.

$$\delta_{ij}^{pc} = -\frac{\beta^2\left(1+p^j\right)\xi^j}{120\left(kT\right)^2}\left[B_0^2\left(\frac{3\cos^2\theta_i - 1}{r_i^3}\right) + \sqrt{6}B_2^2\left(\frac{\sin^2\theta_i \bullet \cos 2\phi_i}{r_i^3}\right)\right]$$
$$= C_j\left(B_0^2 G_i + \sqrt{6}B_2^2 H_i\right) \qquad (4)$$

For lanthanide complexes possessing at least a threefold axis (often abusively called 'axial' systems),[11] $B_2^2 = 0$ and eqn. (4) reduces to eqn. (5) which implies that the magnetic anisotropy and the associated pseudo-contact shifts can be rationally programmed *via* (i) a judicious choice of the lanthanide ion (*via* C_j) and (ii) a precise control of the geometry of the lanthanide coordination sphere (*via* B_0^2).

$$\delta_{ij}^{pc} = C_j B_0^2 G_i \qquad (5)$$

Alternatively, structural variations occurring along the lanthanide series can be easily detected since the ratio δ_{ij}^{pc}/C_j only varies when the pseudo-contact term $B_0^2 G_i$ (and the structure) changes.[10–13] Sophisticated multi-nuclei crystal-field independent methods derived from eqn. (5) have been developed for separating the geometrical term G_i and the crystal-field parameter B_0^2,[14] but the latter approach is limited to the investigation of complexes in which the paramagnetic anisotropy is characterized by a single crystal-field parameter according to Bleaney's approach. In other words, only complexes possessing at least one threefold axis passing through metal ions located on symmetry-equivalent sites can be investigated: a drastic limitation when considering polymetallic lanthanide complexes or rhombic systems in solution.[11,15] In this paper, we report on a simple generalization of the model-free methods for multi-centre paramagnetic lanthanide complexes and its application to the self-assembled homotrimetallic D_3-symmetrical triple-stranded helicates $[Ln_3(L1)_3]^{9+}$ which possess two different metallic sites, and for which the crystal structure of $[Eu_3(L1)_3](CF_3SO_3)_9(CH_3CN)_9(H_2O)_2$ has been reported together with the thermodynamic assembly process occurring in solution (Fig. 1).[16] Particular attention has been focused on the derivation of new crystal-field dependent and independent equations according to Bleaney's approach and their use for detecting structural changes occurring along the lanthanide series in solution.

Results and discussion

Extension of the model-free methods for multi-centre paramagnetic lanthanide complexes

For any nucleus i in a complex of a lanthanide j, the paramagnetic shifts δ_{ij}^{para} are obtained from the experimental chemical shifts δ_{ij}^{exp} by using eqn. (6) if the residual signal of the solvent is taken as an internal reference.[10,11] The diamagnetic contribution δ_i^{dia} in the paramagnetic complexes is obtained from the NMR spectra of the isostructural diamagnetic lanthanum (Ln = Ce–Nd), yttrium (Ln = Sm–Ho) and lutetium (Ln = Er–Yb) complexes.

$$\delta_{ij}^{para} = \delta_{ij}^{exp} - \delta_i^{dia} = \delta_{ij}^{c} + \delta_{ij}^{pc} \qquad (6)$$

The contact contribution δ_{ij}^{c} is given by eqn. (7) and results from spin delocalization according to the Fermi mechanism in which

F_i is the contact term (proportional to the hyperfine Fermi constant A_i) and $\langle S_z\rangle_j$ is the spin expectation values of the S_z operator tabulated by Golding and Halton for the free lanthanide ions at 300 K.[17]

$$\delta_{ij}^{c} = \frac{A_i}{\hbar\gamma_I H_0}\langle S_z\rangle_j = F_i\langle S_z\rangle_j \quad (7)$$

For complexes possessing at least a threefold axis passing through the metal ions, the paramagnetic anisotropy predicted by Bleaney's approach is limited to the axial contribution (eqn. (2)) and the pseudo-contact contribution δ_{ij}^{pc} is given by eqn. (5).[10,11] Substituting eqns. (5) and (7) into eqn. (6) gives eqn. (8) which is well-suited for extracting contact (F_i) and pseudo-contact ($B_0^2G_i$) terms for any nucleus i by a multi-linear least-squares fit of δ_{ij}^{para} *vs.* $\langle S_z\rangle_j$ and C_j along a series of isostructural monometallic lanthanide complexes[13] for which the hyperfine constants and the crystal-field parameter do not vary.[14,15]

$$\delta_{ij}^{para} = F_i\langle S_z\rangle_j + C_jB_0^2G_i \quad (8)$$

The simultaneous consideration of the paramagnetic shifts of two different nuclei i, k in the complex of a lanthanide j provides two equations similar to eqn. (8) (one for the nucleus i and one for the nucleus k) which can be combined to remove the second-rank crystal-field parameter.[11,14] The two-nuclei crystal-field independent eqn. (9) results and structural changes along the lanthanide series can be safely detected since plots of $\frac{\delta_{ij}^{para}}{\langle S_z\rangle_j}$ *vs* $\frac{\delta_{kj}^{para}}{\langle S_z\rangle_j}$ are expected to give straight lines as long as the slope G_i/G_k defined by the ratio of the geometrical factors does not vary.[14,15]

$$\frac{\delta_{ij}^{para}}{\langle S_z\rangle_j} = \left(F_i - F_k\frac{G_i}{G_k}\right) + \frac{G_i}{G_k}\cdot\frac{\delta_{kj}^{para}}{\langle S_z\rangle_j} \quad (9)$$

For multi-centre homopolymetallic lanthanide complexes containing n non-coupled paramagnetic centres located on threefold or fourfold axes, the original monometallic crystal-field dependent eqn. (8) transforms into eqn. (10) according that each Ln^{III} is located at the origin of a specific polar frame (Fig. 2). As discussed for monometallic complexes, multi-linear least-square fits of δ_{ij}^{para} *vs.* $\langle S_z\rangle_j$ and C_j provide contact $\sum_{m=1}^{n} F_i^m$ and pseudo-contact $\sum_{m=1}^{n} B_0^{2m}G_i^m$ terms along an isostructural series, but their interpretation is complicated by the sum over the n paramagnetic sites.[11]

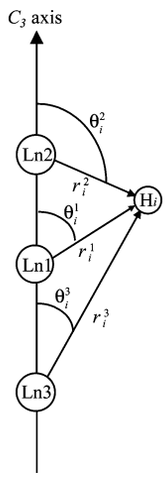

Fig. 2 Axial co-ordinates considered in the trimetallic axial complexes $[Ln_3(L1)_3]^{9+}$. Each Ln^{III} is located at the origin of a specific polar frame.

$$\delta_{ij}^{para} = \left(\sum_{m=1}^{n} F_i^m\right)\langle S_z\rangle_j + \left(\sum_{m=1}^{n} B_0^{2m}G_i^m\right)C_j \quad (10)$$

Further derivation of crystal-field independent methods require the specific expansion of eqn. (10) for each specific case. Since (i) no significant magnetic coupling occurs at room temperature between Ln^{III} ions lying at distance larger than 4 Å[18] (Eu1 ··· Eu2 = 9.3165(7) and Eu1 ··· Eu3 = 9.0762(7) Å in $[Eu_3(L1)_3]^{9+}$)[16] and (ii) the tridentate binding units are separated by methylene spacers in L1 which are poor electronic relays,[15] the contact contributions δ_{ij}^{c} result from through-bond Fermi interactions with a single metallic centre as previously demonstrated for related bimetallic helicates.[15] On the other hand, the pseudo-contact contribution δ_{ij}^{pc} in the D_3-symmetrical helicates $[Ln_3(L1)_3]^{9+}$ results from the sum of the effect induced by each metal ion according to Fig. 2. Different crystal-field parameters are required for the central Ln1–N_9 ($B_0^{2central}$) and the two symmetry-equivalent terminal Ln2–N_6O_3 and Ln3–N_6O_3 ($B_0^{2terminal}$) metallic sites, and eqn. (10) reduces to the one-nucleus crystal-field dependent eqn. (11) for $[Ln_3(L1)_3]^{9+}$.

$$\delta_{ij}^{para} = F_i\langle S_z\rangle_j + (B_0^{2central}G_i^1 + B_0^{2terminal}(G_i^2 + G_i^3))C_j = F_i\langle S_z\rangle_j + S_i\,C_j \quad (11)$$

The simultaneous consideration of three different nuclei i, k and l in $[Ln_3(L1)_3]^{9+}$ provides three equations similar to eqn. (11) from which $B_0^{2central}$ and $B_0^{2terminal}$ can be removed after tedious algebraic transformations to give the multi-centre crystal-field independent eqn. (12) in which the factors B_{ikl}, C_{ikl} and D_{ikl} are given in eqns. (13)–(16).

$$\frac{\delta_{ij}^{para}}{\langle S_z\rangle_j} = B_{ikl} + C_{ikl}\frac{\delta_{kj}^{para}}{\langle S_z\rangle_j} + D_{ikl}\frac{\delta_{lj}^{para}}{\langle S_z\rangle_j} \quad (12)$$

$$B_{ikl} = F_i - F_kC_{ikl} - F_lD_{ikl} \quad (13)$$

$$C_{ikl} = R_{ik}\left(\frac{G_i^1 - G_l^1R_{il}}{G_k^1R_{ik} - G_l^1R_{il}}\right) \quad (14)$$

$$D_{ikl} = -R_{il}\left(\frac{G_i^1 - G_k^1R_{ik}}{G_k^1R_{ik} - G_l^1R_{il}}\right) \quad (15)$$

$$R_{xy} = \left(\frac{G_x^2 + G_x^3}{G_y^2 + G_y^3}\right) \quad (16)$$

Eqn. (12) corresponds to the equation of a plane perpendicular to the vector $(1, -C_{ikl}, -D_{ikl})$ and separated by a distance B_{ikl} from the origin in a homogeneous 3D space in which $\frac{\delta_{ij}^{para}}{\langle S_z\rangle_j}$, $\frac{\delta_{kj}^{para}}{\langle S_z\rangle_j}$ and $\frac{\delta_{ij}^{para}}{\langle S_z\rangle_j}$ define the orthogonal x, y and z directions. The structural factors C_{ikl} and D_{ikl} are complicated non-linear combinations of the geometrical factors G_i^m, G_k^m and G_l^m (m = 1–3), but any deviation of the triplets $\frac{\delta_{ij}^{para}}{\langle S_z\rangle_j}$, $\frac{\delta_{kj}^{para}}{\langle S_z\rangle_j}$, $\frac{\delta_{ij}^{para}}{\langle S_z\rangle_j}$ from the plane along the lanthanide series affects C_{ikl} and D_{ikl} and implies a structural change occurring in the lanthanide helicates $[Ln_3(L1)_3]^{9+}$. The variation of the B_{ikl} factor is more difficult to interpret since the contact terms F_i, F_k and F_l

Table 1 Experimental and computed ^{1}H NMR shifts (in ppm with respect to $SiMe_4$) for $[Ln_3(L1)_3]^{9+}$ in CD_3CN at 298 K [a]

Compound	H1	H2	H3	H4	H5	H6	H7	H8	H9	H10	H11	Me17	Me18	Me19	Me20
L1	8.37	8.30	8.00	7.91	7.71	7.69	7.51	7.34	7.22	7.33	7.22	1.31	1.42	1.04	1.25
$[La_3(L1)_3]^{9+}$	8.20	7.64	8.09	8.18	5.88	5.76	7.60	7.53	6.92	7.19	7.24	1.42	1.39	0.65	0.90
$[Y_3(L1)_3]^{9+}$	8.27	7.55	7.92	8.17	5.50	5.32	7.65	7.51	6.87	7.22	7.19	1.46	1.44	0.59	1.01
$[Lu_3(L1)_3]^{9+}$	8.28	7.53	7.88	8.17	5.39	5.19	7.66	7.50	6.89	7.24	7.16	1.45	1.44	0.58	1.04
$[Ce_3(L1)_3]^{9+}$	10.27	8.19	8.71	9.78	−2.17	−2.40	8.87	7.47	6.27	7.14	6.79	2.46	1.78	−2.44	1.05
$[Ce_3(L1)_3]^{9+\,b}$	9.95	8.11	8.70	9.68	−1.66	−1.91	8.80	7.49	6.29	7.09	6.78	2.38	2.74	−2.43	1.15
$[Pr_3(L1)_3]^{9+}$	11.76	9.73	9.63	10.62	−8.75	−9.60	9.68	7.78	5.77	7.21	6.39	3.09	2.00	−4.74	1.27
$[Pr_3(L1)_3]^{9+\,b}$	11.59	8.93	9.36	10.90	−7.78	−8.31	9.89	7.82	5.78	7.14	6.40	3.11	2.02	−4.86	1.37
$[Nd_3(L1)_3]^{9+}$	10.51	9.80	9.43	9.57	−1.31	−2.73	9.12	8.16	6.29	7.51	6.79	2.10	1.12	−2.00	1.12
$[Nd_3(L1)_3]^{9+\,b}$	10.38	9.39	9.12	9.48	−0.62	−1.41	9.01	8.57	6.35	7.50	6.82	2.11	1.66	−1.82	1.15
$[Eu_3(L1)_3]^{9+}$	4.76	4.17	6.21	6.35	13.10	14.04	5.24	4.50	7.62	6.35	7.76	0.71	0.84	3.61	0.53
$[Eu_3(L1)_3]^{9+\,b}$	4.51	3.48	5.90	6.44	14.14	15.58	5.29	4.73	7.66	6.29	7.78	0.71	1.11	3.64	0.63
$[Tb_3(L1)_3]^{9+}$	20.20	−3.14	8.86	25.20	−80.00	−75.00	16.80	−5.57	0.12	1.42	2.27	13.91	5.80	−36.50	3.50
$[Tb_3(L1)_3]^{9+\,b}$	20.24	−3.04	8.89	25.18	−80.15	−75.19	16.79	−5.14	0.11	1.43	2.27	13.91	5.78	−36.49	3.48
$[Dy_3(L1)_3]^{9+}$	24.50	−6.80	3.90	26.30	−100.0	−90.0	18.54	−5.86	0.50	3.80	1.86	15.72	14.80	−41.60	11.20
$[Dy_3(L1)_3]^{9+\,b}$	23.58	−6.70	3.34	25.90	−104.1	−100.9	18.44	−6.05	−1.06	2.35	2.25	15.79	14.79	−43.08	11.52
$[Ho_3(L1)_3]^{9+}$	14.39	−2.25	3.81	17.10	−55.00	−55.00	12.15	−2.25	0.95	2.20	5.55	9.87	7.67	−23.50	7.30
$[Ho_3(L1)_3]^{9+\,b}$	16.33	−2.31	4.58	17.03	−45.93	−34.95	12.22	−1.92	4.04	4.63	4.92	9.82	7.58	−20.67	6.48
$[Er_3(L1)_3]^{9+}$	9.17	3.19	5.79	4.67	30.00	51.00	4.67	3.19	12.00	7.96	7.96	2.87	−1.24	7.40	−0.34
$[Er_3(L1)_3]^{9+\,b}$	7.73	2.96	6.05	6.50	22.87	42.78	4.88	3.04	10.08	7.37	8.07	2.69	−0.96	5.87	0.54
$[Tm_3(L1)_3]^{9+}$	3.97	6.25	7.85	4.37	45.00	69.00	2.93	6.25	11.21	8.94	8.94	−0.71	−3.60	15.05	−1.31
$[Tm_3(L1)_3]^{9+\,b}$	4.41	6.36	7.16	2.71	45.89	63.88	2.68	6.28	11.63	8.43	9.10	−0.53	−3.74	15.14	−1.74
$[Yb_3(L1)_3]^{9+}$	6.19	6.93	7.60	6.44	17.00	19.00	5.61	7.38	8.59	7.93	7.88	0.37	−0.48	6.57	0.07
$[Yb_3(L1)_3]^{9+\,b}$	6.52	7.35	7.69	5.76	22.82	29.47	5.57	7.28	8.84	7.78	7.99	0.43	−0.78	6.92	−0.21

[a] Sm^{III} is not considered because of its weak paramagnetism. [b] Chemical shifts calculated with eqn. (11).

and the structural factors C_{ikl} and D_{ikl} are involved. Consequently, a translation of the plane along the lanthanide series cannot be systematically assigned to a structural change because the variation of the Fermi constants is sufficient for affecting B_{ikl} without changing C_{ikl} and D_{ikl}. Related translations of the intercept $F_i - F_k(G_i/G_k)$ according to eqn. (9) in a 2D space have been reported for isostructural monometallic complexes.[11,14] Finally, eqns. (14)–(16) can be used for comparing the solution structure of $[Ln_3(L1)_3]^{9+}$ with structural models obtained in the solid state or in the gas phase since the axial coordinates of the nuclei *i*,*k*,*l* allow the *a priori* calculations of C_{ikl} and D_{ikl} (the threefold axis of the complex being taken as the principal magnetic *z* axis, Fig. 2).[15,19]

Diamagnetic ^{1}H NMR spectra and solution structures of $[Ln_3(L1)_3]^{9+}$ (Ln = La, Y, Lu)

The ^{1}H NMR spectra of $[Ln_3(L1)_3]^{9+}$ for the diamagnetic metals Ln = La, Y, Lu display 25 well-resolved signals which can be assigned by using {^{1}H–^{1}H}-COSY and {^{1}H–^{1}H}-NOESY to 11 aromatic protons (H1–H11), 10 methylene protons (H12–H16) and 4 methyl groups (Me17–Me20) characteristic of a half ligand strand and pointing to average D_3, D_{3h} or C_{3h} symmetry for the complexes in solution (Fig. 3a, Table 1). The assignment of these specific diamagnetic NMR data to a racemic mixture of triple-stranded helicates with average D_3-symmetry has been described in a preliminary communication,[16] but some points merit to be briefly repeated here and further discussed to provide a complete structural characterization of $[Ln_3(L1)_3]^{9+}$ in solution. The systematic diastereotopicity of all methylene protons (H12–H16) (observed as pseudo-sextets because $^2J \approx 2(^3J)$, Fig. 3a) excludes a D_{3h} symmetrical arrangement of the three strands (*i.e.* a non-helical arrangement or a fast helical interconversion), but it is compatible with a non-interconverting racemic mixture of (i) helicates *PPP*-$[Ln_3(L1)_3]^{9+}$ and *MMM*-$[Ln_3(L1)_3]^{9+}$ or (ii) side-by-side complexes *PMP*-$[Ln_3(L1)_3]^{9+}$ and *MPM*-$[Ln_3(L1)_3]^{9+}$ belonging to the D_3 point group.[20]

The large upfield complexation shifts of the protons bound to the 4-position of the benzimidazole rings (H5,H6) in $[La_3(L1)_3]^{9+}$ ($\Delta\delta$ = 1.83–1.93 ppm), $[Y_3(L1)_3]^{9+}$ ($\Delta\delta$ = 2.21–2.37 ppm) and $[Lu_3(L1)_3]^{9+}$ ($\Delta\delta$ = 2.32–2.50 ppm, Table 1) are diagnostic for a regular helication which puts these protons in the shielding region of the connected benzimidazole ring[21] in agreement with the crystal structure of $[Eu_3(L1)_3]^{9+}$ (Fig. 1), but in complete contradiction with amphiverse *PMP* (or *MPM*) conformers. The observation of weak but significant interstrand NOE effects (for instance H9–Me17) points to three strands tightly wrapped about the helical axis,[21] which rules out complexes possessing a central lanthanide with no helicity such as the racemic mixture of *P*–*P*-$[Ln_3(L1)_3]^{9+}$ and *M*–*M*-$[Ln_3(L1)_3]^{9+}$ (D_3-symmetry) or the side-by-side complex *P*–*M*-$[Ln_3(L1)_3]^{9+}$ (C_{3h}-symmetry). These NMR data unambiguously establish that (i) the triple-helical structure observed in the solid state is maintained in solution along the complete lanthanide series and (ii) that relaxation of intermolecular constraints provides a racemic mixture of inert triple-stranded helicates *PPP*-$[Ln_3(L1)_3]^{9+}$ and *MMM*-$[Ln_3(L1)_3]^{9+}$ with average D_3-symmetry on the NMR time scale.

Assignment of the ^{1}H NMR spectra for the weakly paramagnetic helicates $[Ln_3(L1)_3]^{9+}$ (Ln = Ce, Pr, Nd, Sm, Eu, Tm, Yb)

The ^{1}H NMR spectra of the paramagnetic complexes $[Ln_3(L1)_3]^{9+}$ (Ln = Ce–Yb except Pm and Gd) display 25 signals in agreement with the D_3-symmetry exhibited by the analogous diamagnetic complexes. A reliable assignment depends on the detection of ^{1}H–^{1}H scalar (*via* COSY spectra) and ^{1}H–^{1}H dipolar couplings (*via* NOESY spectra) which is limited by the increased nuclear relaxation induced by the electronic spin.[22] Since the lanthanide-induced paramagnetic nuclear relaxation for fast-relaxing lanthanides is dominated by dipolar interactions, eqns. (17) and (18) hold for a single paramagnetic centre[10,11] and long longitudinal (T_1) and transverse (T_2) relaxation suitable for COSY and NOESY experiments[22] only exist for weakly paramagnetic Ln^{III} (*i.e.* possessing small magnetic moments μ_{eff}) displaying short electronic (τ_e) and rotational (τ_r) correlations times (H_0 is the applied magnetic field, the other terms have their usual meaning). A complete assignment is thus only obtained for $[Ln_3(L1)_3]^{9+}$ with Ln = Ce, Pr, Nd, Sm, Eu, Tm, Yb (Table 1, Fig. 3b,c), while broad signals without significant cross peaks in 2D-spectra are obtained for Ln = Tb–Er.

$$\frac{1}{T_{1i}^{para}} = \frac{4}{3}\left(\frac{\mu_0}{4\pi}\right)^2 \frac{\gamma_I \mu_{eff}^2 \beta^2}{r_i^6}\tau_e + \frac{6}{5}\left(\frac{\mu_0}{4\pi}\right)^2 \frac{\gamma_I^2 \mu_{eff}^4 \beta^4 H_0^2}{r_i^6 (3kT)^2}\left(\frac{\tau_r}{1+\omega_I^2\tau_r^2}\right) \quad (17)$$

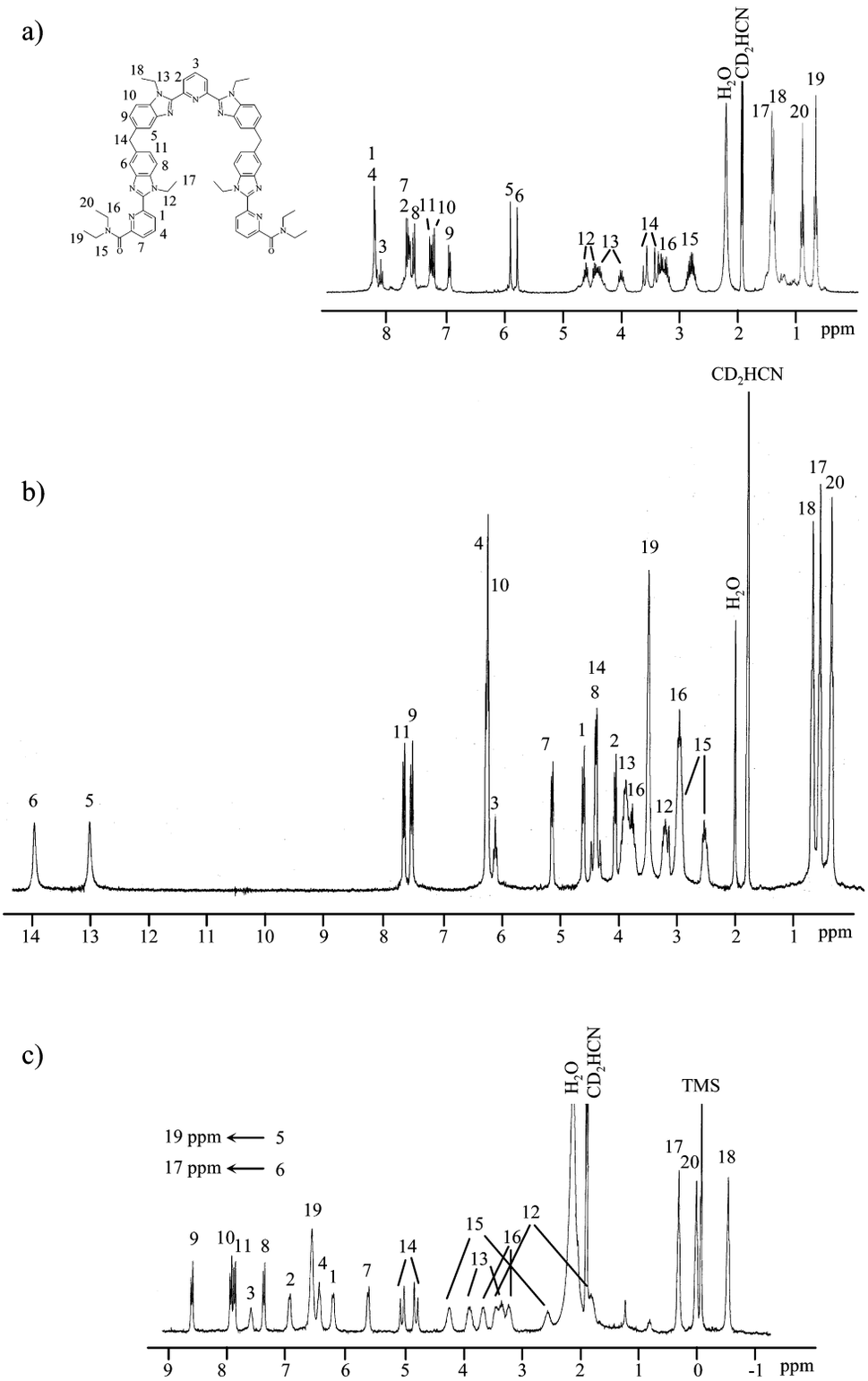

Fig. 3 ^{1}H NMR spectra of a) $[La_3(L1)_3]^{9+}$, b) $[Eu_3(L1)_3]^{9+}$ and c) $[Yb_3(L1)_3]^{9+}$ in CD_3CN (298 K).

Since each multiplet of the diastereotopic methylene protons (H12–H16) cannot be assigned unambiguously to one specific proton of the pair,[23] these signals are not considered for further structural analyses by using paramagnetic NMR methods. However, only elusive NOE effects can be detected between the aromatic protons H8 and H10 and the adjacent ethyl residues, which prevents a definitive assignment of the methyl groups Me17–Me20. In order to overcome this limitation, we have resorted to the determination of the longitudinal paramagnetic relaxation rates $1/T_{1i}^{para}$ for i = Me17–Me20 in the paramagnetic helicates $[Ln_3(L1)_3]^{9+}$ (Ln = Ce–Eu). Since (i) both static and transcient dipolar contributions depend on r_i^{-6} (eqn. (17)),[23] and (ii) the three paramagnetic centres are not magnetically coupled, $1/T_{1i}^{para}$ is given by the sum of three independent contributions originating from each paramagnetic centre, and eqn. (19) holds for the homotrimetallic helicates $[Ln_3(L1)_3]^{9+}$ in which E_j is an experimental magnetic constant ($\mu_{eff}^m = \mu_{eff}$ (m = 1–3) in which μ_{eff} is the magnetic moment for an isolated paramagnetic centre).

Taking the D_3-average Ln–H distances (r_i^m, m = 1–3; Fig. 2) measured in the crystal structure of $[Eu_3(L1)_3](CF_3SO_3)_9(CH_3CN)_9(H_2O)_2$ for Me17–Me20,[16] the $\sum_{m=1}^{3} \frac{1}{\left(r_i^m\right)^6}$ terms can be

$$\frac{1}{T_{2i}^{\text{para}}} = \frac{4}{3}\left(\frac{\mu_0}{4\pi}\right)^2 \frac{\gamma_I \mu_{\text{eff}}^2 \beta^2}{r_i^6}\tau_e + \frac{1}{5}\left(\frac{\mu_0}{4\pi}\right)^2 \frac{\gamma_I^2 \mu_{\text{eff}}^4 \beta^4 H_0^2}{r_i^6 (3kT)^2}\left(4\tau_r + \frac{3\tau_r}{1+\omega_I^2\tau_r^2}\right) \quad (18)$$

$$\frac{1}{T_{1i}^{\text{para}}} = \sum_{m=1}^{3}\left[\frac{4}{3}\left(\frac{\mu_0}{4\pi}\right)^2 \frac{\gamma_I \left(\mu_{\text{eff}}^m\right)^2 \beta^2}{\left(r_i^m\right)^6}\tau_e + \frac{6}{5}\left(\frac{\mu_0}{4\pi}\right)^2 \frac{\gamma_I^2 \left(\mu_{\text{eff}}^m\right)^4 \beta^4 H_0^2}{\left(r_i^m\right)^6 (3kT)^2}\left(\frac{\tau_r}{1+\omega_I^2\tau_r^2}\right)\right] = E_j \cdot \sum_{m=1}^{3}\frac{1}{\left(r_i^m\right)^6} \quad (19)$$

calculated. Among all the possible permutations of the methyl groups Me17–Me20 for a given helicate $[Ln_3(L1)_3]^{9+}$, only a single plot of $1/T_{1i}^{\text{para}}$ *vs.* $\sum_{m=1}^{3}\frac{1}{\left(r_i^m\right)^6}$ displays a satisfying linear correlation according to eqn. (19), which leads to the unambiguous assignment of the methyl groups collected in Table 1 (Fig. S1, ESI).

Application of the one-nucleus multi-centre crystal-field dependent method (eqn. (11)) and assignment of the ^{1}H NMR spectra for the strongly paramagnetic helicates $[Ln_3(L1)_3]^{9+}$ (Ln = Tb, Dy, Ho, Er)

The two linear forms (eqns. (20) and (21), $S_i = (B_0^{2\text{central}} G_i^1 + B_0^{2\text{terminal}}(G_i^2 + G_i^3))$) derived from the crystal-field dependent eqn. (11) can be used for testing isostructurality along the lanthanide series for $[Ln_3(L1)_3]^{9+}$, since plots of $\frac{\delta_{ij}^{\text{para}}}{\langle S_z\rangle_j}$ *vs.* $\frac{C_j}{\langle S_z\rangle_j}$ (eqn. (20)) and $\frac{\delta_{ij}^{\text{para}}}{C_j}$ *vs.* $\frac{\langle S_z\rangle_j}{C_j}$ (eqn. (21)) are expected to give linear correlations as long as the structural factors G_i^m (m = 1–3), the contact term F_i and the crystal-field parameters $B_0^{2\text{central}}$ and $B_0^{2\text{terminal}}$ do not change along the lanthanide series.[11,23]

$$\frac{\delta_{ij}^{\text{para}}}{\langle S_z\rangle_j} = F_i + S_i\frac{C_j}{\langle S_z\rangle_j} \quad (20)$$

$$\frac{\delta_{ij}^{\text{para}}}{C_j} = S_i + F_i\frac{\langle S_z\rangle_j}{C_j} \quad (21)$$

These plots are linear for the aromatic protons (H1–H11) and the methyl groups (Me17–Me20) for the light lanthanides (Ln = Ce–Eu) for which the ^{1}H NMR spectra have been fully assigned, in agreement with the existence of a single structure in solution (Fig. 4). A first set of F_i and S_i terms, obtained by multi-linear least-squares fits of eqn. (11), have been used for the prediction of the ^{1}H NMR spectra of $[Ln_3(L1)_3]^{9+}$ with the smaller lanthanides (Ln = Tb–Yb).[24] Comparison between predictions and experimental data is only satisfying for $[Tb_3(L1)_3]^{9+}$, thus allowing a complete assignment for this complex (Table 1) and its consideration for the calculation of the final set of F_i and S_i terms for the first series (Ln = Ce–Tb, Table 2).

Quantitative comparisons of the experimental paramagnetic shifts with those calculated with eqn. (11) for the first series Ln = Ce–Tb (Table 1) are given by the Wilcott agreement factors[25] which are acceptable for all aromatic and methyl protons ($0.01 < AF_i < 0.18$, Table 2). They can be compared with similar mathematical treatments previously applied to monometallic complexes which are structural models of the central ($[Ln(L2)_3]^{3+}$; $0.04 < AF_i < 0.25$)[26] and of the terminal ($[LnCo(L3)_3]^{6+}$; $0.01 < AF_i < 0.20$)[23] metallic sites in $[Ln_3(L1)_3]^{9+}$ (Fig. 5).

The F_i values are negligible for protons separated from the paramagnetic centre by more than five bonds, thus justifying that the contact contribution can be limited to a single magnetic centre in $[Ln_3(L1)_3]^{9+}$. Interestingly, the absolute values $|F_i|$ for

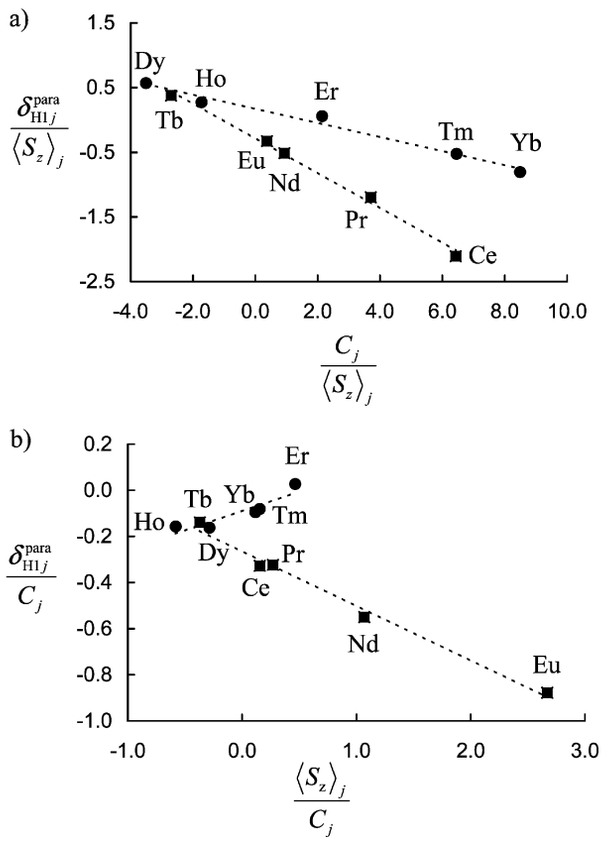

Fig. 4 Plots of a) $\frac{\delta_{ij}^{\text{para}}}{\langle S_z\rangle_j}$ *vs.* $\frac{C_j}{\langle S_z\rangle_j}$ (eqn. (20)) and b) $\frac{\delta_{ij}^{\text{para}}}{C_j}$ *vs.* $\frac{\langle S_z\rangle_j}{C_j}$ eqn. (21)) for H1 in $[Ln_3(L1)_3]^{9+}$ (Ln = Ce–Yb, except Pm and Gd, CD_3CN, 298 K).

the pyridine protons H2 (H_{meta}: $F_{H2} = -0.38$) and H3 (H_{para}: $F_{H3} = -0.16$) of the central site are larger than those found for the related pyridine protons of the terminal sites H1 and H7 (H_{meta}: $F_{H1} = -0.26$, $F_{H7} = -0.16$) and H4 (H_{para}: $F_{H4} = -0.08$) respectively, which strongly suggests a larger spin delocalization onto the central tridentate bis(benzimidazole)pyridine units. These results closely parallel the F_i values obtained for $[Ln(L2)_3]^{3+}$ ($F_{H5} = -0.42$, $F_{H6} = -0.26$),[26] the model for the central LnN_9 metallic site, whose absolute values are larger than those found in $[LnCo(L3)_3]^{6+}$ ($F_{H12} = -0.24$, $F_{H14} = -0.17$ and $F_{H13} = -0.09$),[23] the model for the terminal LnN_6O_3 metallic sites. The unsymmetrical delocalization $|F_{H1}| > |F_{H7}|$ in $[Ln_3(L1)_3]^{9+}$ parallels $|F_{H12}| > |F_{H14}|$ found for $[LnCo(L3)_3]^{6+}$ which is characteristic for co-ordinated NNO tridentate binding units.[23] The pseudo-contact terms S_i are difficult to interpret because they combine two crystal-field and three geometrical parameters. The maximum absolute values found for H5 and H6 confirm the tight helical wrapping of the strands which forces them to point inside the triple helix and close to the metal ions (*i.e.* $(r_i^m)^{-3}$ are large).

The larger absolute values of S_i observed for H1, H4, H7 compared with those obtained for the central pyridine (H2–H3)

Table 2 Computed values for contact (F_i) and pseudo-contact $S_i = (B_0^{2\text{central}}G_i^1 + B_0^{2\text{terminal}}(G_i^2 + G_i^3))$ terms and agreement factors (AF_i) for aromatic and methyl protons in complexes $[Ln_3(L1)_3]^{9+}$ (CD_3CN, 298 K)[a]

Compound	H1	H2	H3	H4	H5	H6	H7	H8	H9	H10	H11	Me17	Me18	Me19	Me20
Ln = Ce–Tb															
F_i	−0.26(2)	−0.38(4)	−0.16(2)	−0.08(1)	0.38(6)	0.54(9)	−0.16(1)	−0.28(2)	0.039(3)	−0.098(3)	0.030(1)	0.014(3)	−0.01(2)	0.11(1)	−0.02(1)
S_i	−0.24(1)	−0.02(2)	−0.07(1)	−0.23(1)	1.14(2)	1.13(4)	−0.17(1)	0.05(1)	0.093(1)	0.031(2)	0.068(1)	−0.150(2)	−0.054(9)	0.471(3)	−0.037(6)
AF_i[b]	0.03	0.10	0.18	0.02	0.02	0.03	0.03	0.04	0.01	0.02	0.01	0.01	0.14	0.01	0.07
Ln = Dy–Yb															
F_i	0.18(4)	−0.37(1)	−0.13(1)	0.17(4)	−0.8(2)	0.1(5)	0.03(1)	−0.36(1)	0.02(7)	−0.06(5)	−0.03(1)	0.24(1)	0.08(1)	−0.37(6)	0.19(2)
S_i	−0.10(1)	0.036(3)	0.01(1)	−0.13(1)	0.88(7)	1.1(2)	−0.099(2)	0.033(2)	0.09(2)	0.03(2)	0.041(4)	−0.075(2)	−0.103(3)	0.33(2)	−0.071(8)
AF_i[b]	0.15	0.03	0.20	0.12	0.10	0.19	0.03	0.02	0.36	0.46	0.14	0.02	0.03	0.07	0.11

[a] F_i and S_i are obtained by multi-linear least-squares fits of $\delta_{ij}^{\text{para}}$ *vs.* $\langle S_{zj}\rangle$ and C_j (eqn. (11), see text). [b] Calculated according to[25] $AF_i = \sqrt{\frac{\sum_j \left(\delta_{ij}^{\text{obs}} - \delta_{ij}^{\text{calc}}\right)^2}{\sum_j \left(\delta_{ij}^{\text{obs}}\right)^2}}$

are responsible for the stronger paramagnetic shift experienced by the terminal pyridine ring, but its eventual assignment to specific geometrical parameters requires the evaluation of the crystal-field parameters. Taking the crystal structure of $[Eu_3(L1)_3]^{9+}$ as a structural model for the solution structure, the geometrical factors G_i^m (m = 1–3) can be calculated (Table 3) and a multi-linear least-squares fit of S_i *versus* G_i^1 and $G_i^2 + G_i^3$ for the eleven aromatic protons H1–H11 gives $B_0^{2\text{central}} = -45(3)$ and $B_0^{2\text{terminal}} = -67(3)$.[27] The quality of the linear correlation is satisfying leading to an agreement factor AF_S = 0.07 between calculated and experimental S_i factors which strongly suggests that only minor structural changes occur between the solid-state and the solution structures in these rigid polymetallic helicates as previously established for bimetallic d–f[23] and f–f[15] helicates. We can now rationalize the origin of the larger values observed for $|S_{H1}|$, $|S_{H4}|$, $|S_{H7}|$ compared to $|S_{H2}|$, $|S_{H3}|$ which result from a combination of (i) the larger crystal-field effects associated with the terminal sites ($|B_0^{2\text{terminal}}| > |B_0^{2\text{central}}|$) and (ii) the larger compensation effect resulting from opposite paramagnetic contributions for the central metallic site (*i.e.* G_i^1 and $G_i^2 + G_i^3$ display opposite signs for all pyridine protons, but the absolute values of the ratios $|B_0^{2\text{central}}G_i^1/B_0^{2\text{terminal}}(G_i^2 + G_i^3)| = 1.7–1.8$ are smaller for H2–H3 than $|B_0^{2\text{terminal}}(G_i^2 + G_i^3)/B_0^{2\text{central}}G_i^1| = 5.8–6.9$ for H1, H4 and H7, Table 3).

The deviation from linearity according to eqns. (20) and (21) observed for the two helicates $[Ln_3(L1)_3]^{9+}$ with the heavy lanthanides Ln = Tm, Yb (for which a complete assignment of the ^{1}H NMR spectra is accessible from dipolar and scalar couplings, Fig. 4), indicates that an abrupt structural and/or crystal-field change occurs near the middle of the lanthanide series. Taking the paramagnetic shifts measured for $[Ln_3(L1)_3]^{9+}$ (Ln = Tm, Yb) as the two first points of a second isostructural series, a set of F_i and S_i terms can be calculated by multi-linear least-squares fits of eqn. (11). Subsequent predictions of the ^{1}H NMR spectra for $[Ln_3(L1)_3]^{9+}$ (Ln = Dy–Er) show satisfying correlations between calculated and experimental spectra, thus allowing (i) a complete assignment of the NMR spectra for the heavy lanthanides (Table 1) and (ii) the calculation of a second final set of F_i and S_i terms for the second isostructural series (Ln = Dy–Yb, Table 2, Fig. 4). The Wilcott agreement factors (AF_i, Table 2) for Ln = Dy–Yb are comparable with those found for Ln = Ce–Tb, except for AF_{H9} = 0.36 and AF_{H10} = 0.46 exhibiting inaccurate F_i terms. The general trends in the F_i and S_i terms previously discussed for Ln = Ce–Tb also hold for Ln = Dy–Yb and the change of the Fermi constants occurring near the middle of the lanthanide series for $[Ln_3(L1)_3]^{9+}$ is reminiscent of similar behaviours reported for monometallic complexes, although their origins remain obscure.[11,14,19] The abrupt change of the pseudo-contact S_i terms near the middle of the lanthanide series, often refered to as the 'gadolinium break' results from the decrease of the interaction between the donor atoms of the ligands and Ln^{III} when the spatial diffuseness of the 4f electronic orbitals is reduced.[5,28,29] Although this change is expected to be smooth along the lanthanide series,[5,29] the abrupt increase of the sensitivity of magnetic anisotropy to crystal-field effects for the heavy lanthanides (*i.e.* Bleaney's factors C_j in eqn. (4) become very large for Ln = Tb–Yb)[12] amplifies minor variations of the crystal-field parameters or of the geometrical G_i terms.[30] Therefore, the apparent abrupt changes of S_i near the middle of the lanthanide series do not necessarily involve significant structural changes,[11] and the application of crystal-field independent methods in the next section indeed unambiguously demonstrates that isostructurality occurs along the complete lanthanide series for $[Ln_3(L1)_3]^{9+}$. We have thus again resorted to the geometrical factors G_i^m (m = 1–3) calculated from the crystal structure of $[Eu_3(L1)_3]^{9+}$ (Table 3) for estimating the crystal-field parameters $B_0^{2\text{central}} = -33(5)$ and $B_0^{2\text{terminal}} = -61(5)$ for the heavy lanthanides (Ln = Dy–Yb;

Table 3 Geometrical factors G_l^1 and $G_l^2 + G_l^3$ for the aromatic protons H1–H11 calculated in the crystal structure of $[Eu_3(L1)_3](CF_3SO_3)_9(CH_3CN)_9(H_2O)_2$ ($G_l^{m\text{solid}}$), and in solution ($G_l^{m\text{solution}}$) with eqns. (22) and (23) for $[Ln_3(L1)_3]^{9+}$ (CD_3CN, 298 K)

Proton	$G_l^{1\text{solid}}$	$G_l^{2\text{solid}} + G_l^{3\text{solid}}$	$G_l^{1\text{solution}}$	$G_l^{2\text{solution}} + G_l^{3\text{solution}}$
H1	-1.07×10^{-3}	5.05×10^{-3}	9.82×10^{-3}	-5.21×10^{-4}
H2	5.19×10^{-3}	-2.00×10^{-3}	3.08×10^{-3}	-1.70×10^{-3}
H3	3.88×10^{-3}	-1.48×10^{-3}	[a]	[a]
H4	-7.00×10^{-4}	3.29×10^{-3}	6.78×10^{-3}	5.42×10^{-4}
H5	-1.45×10^{-2}	-6.66×10^{-3}	-2.49×10^{-2}	-1.20×10^{-2}
H6	-5.41×10^{-3}	-1.35×10^{-2}	-1.28×10^{-2}	-2.16×10^{-2}
H7	-7.96×10^{-4}	3.16×10^{-3}	4.09×10^{-3}	1.14×10^{-3}
H8	-8.71×10^{-4}	-8.91×10^{-6}	-1.28×10^{-3}	-3.98×10^{-4}
H9	-2.70×10^{-4}	-9.92×10^{-4}	-5.87×10^{-4}	-1.94×10^{-3}
H10	9.60×10^{-4}	-1.39×10^{-3}	[a]	[a]
H11	-5.10×10^{-4}	-1.12×10^{-3}	-1.63×10^{-3}	-3.90×10^{-4}

[a] The G_l^1 and $G_l^2 + G_l^3$ for H3 and H10 in the crystal structure of $[Eu_3(L1)_3](CF_3SO_3)_9(CH_3CN)_9(H_2O)_2$ have been taken as references for calculating the related geometrical factors in solution for the remaining aromatic protons.

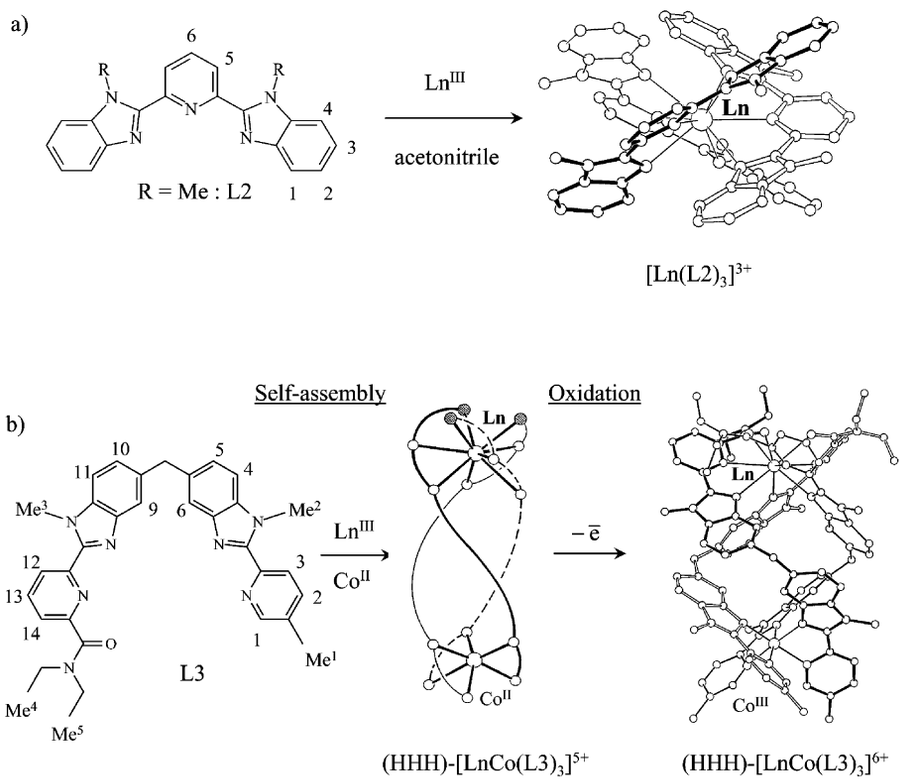

Fig. 5 a) Schematic formation of the D_3-symmetrical complexes $[Ln(L2)_3]^{3+}$ in acetonitrile with numbering scheme. The representation of $[Ln(L2)_3]^{3+}$ corresponds to the crystal structure of $[Eu(L2)_3](ClO_4)_3$ [44] which is considered as a model for the central metallic site in $[Ln_3(L1)_3]^{9+}$. b) Self-assembly of the C_3-symmetrical (HHH)-$[LnCo^{II}(L3)_3]^{5+}$ helicate followed by oxidation (post-modification) to give (HHH)-$[LnCo^{III}(L3)_3]^{6+}$. The representation of $[LnCo(L3)_3]^{6+}$ corresponds to the crystal structure of $[LaCo(L3)_3](ClO_4)_{5.5}(OH)_{0.5}(CH_3CN)_4(H_2O)_2$ [23] in which the lanthanide site is considered as a model for the terminal metallic sites in $[Ln_3(L1)_3]^{9+}$.

multi-linear least-squares fit of S_i *versus* G_i^1 and $G_i^2 + G_i^3$ for the eleven aromatic protons H1–H11 in $[Ln_3(L1)_3]^{9+}$, $AF_S = 0.25$).

The concomitant decrease of $B_0^{2\text{central}}$ and $B_0^{2\text{terminal}}$ when going from large (Ln = Ce–Tb) to small Ln^{III} (Ln = Dy–Yb) matches the expected trend [5,11,28,29] and the ratios

$$\frac{B_0^{2\text{central}}(\text{R} = \text{Ce–Tb})}{B_0^{2\text{central}}(\text{R} = \text{Dy–Yb})} = 1.4(2)$$

and

$$\frac{B_0^{2\text{terminal}}(\text{R} = \text{Ce–Tb})}{B_0^{2\text{terminal}}(\text{R} = \text{Dy–Yb})} = 1.1(2)$$

can be compared with $\frac{B_0^2(\text{R} = \text{Ce–Eu})}{B_0^2(\text{R} = \text{Tb–Yb})} = 1.6(2)$ reported for the triple-stranded d–f helicates $[LnCo(L3)_3]^{6+}$,[23] and $\frac{B_0^2(\text{R} = \text{Ce–Eu})}{B_0^2(\text{R} = \text{Tb–Yb})} = 1.5(1)$ found for $[Ln(2,6\text{-dipicolinate})_3]^{3-}$.[19]

Interestingly, the break always occurs around Gd^{III}, and the subsequent Tb^{III}-complexes correspond to pivots which can be assigned indifferently to either series without significantly affecting the results of the mathematical treatment using eqn. (11).

Application of the three-nuclei multi-centre crystal-field independent method (eqn. (12))

The crystal-field independent eqn. (12) requires the combination of three nuclei *i*, *k*, *l* for investigating isostructurality for $[Ln_3(L1)_3]^{9+}$ along the lanthanide series. Since the structural factors C_{ikl} (eqn. (14)) and D_{ikl} (eqn. (15)) are complicated non-linear functions of the geometrical parameters G_i^m (m = 1–3), there is no straightforward transformation for obtaining *C* and *D* factors with a specific *ikl* ordering from the other five permutations. 2730 ordered H*ikl* triplets (and 2730 associated planes according to eqn. (12)) are thus required for exhaustively characterizing the solution structure of $[Ln_3(L1)_3]^{9+}$ if eleven aro-

matic protons (H1–H11) and four methyl groups (Me17–Me20) are considered. In order to restrict the number of investigated triplets to a representative sample containing the minimal structural information, we have fixed that $i < k < l$ which leads to 455 triplets of which only 165 correspond to triplets exclusively made of aromatic protons for which the positions in the complex are well-defined in the solid state and solution. 3D plots of $\frac{\delta_{ij}^{para}}{\langle S_z \rangle_j}$ *vs.* $\frac{\delta_{kj}^{para}}{\langle S_z \rangle_j}$ and $\frac{\delta_{ij}^{para}}{\langle S_z \rangle_j}$ for the 165 aromatic H*ikl* triplets (H1–H11) systematically show the experimental points to be aligned in a plane, in agreement with the existence of a single D_3-symmetrical triple-helical structure in solution (Fig. 6). Surprisingly, the B_{ikl} parameters, which depend on the contact terms (F_i, F_k and F_l), should display an abrupt change near the middle of the lanthanide series because the one-nucleus crystal-field dependent method (eqn. (11)) indicates that F_i changes between Ln = Ce–Tb and Ln = Dy–Yb (Table 2). Graphically, B_{ikl} corresponds to the distance between the plane and the origin and we thus expect two parallel planes for Ln = Ce–Tb and Ln = Dy–Yb respectively. This is never observed for the 165 H*ikl* triplets (as shown, *e.g.*, in Fig. 6 for H1,2, 3), which suggests that compensation effects prevent B_{ikl} to be sensitive to the variation of the Fermi constants as previously discussed for monometallic,[19] and bimetallic lanthanide complexes (eqn. (9)).[15]

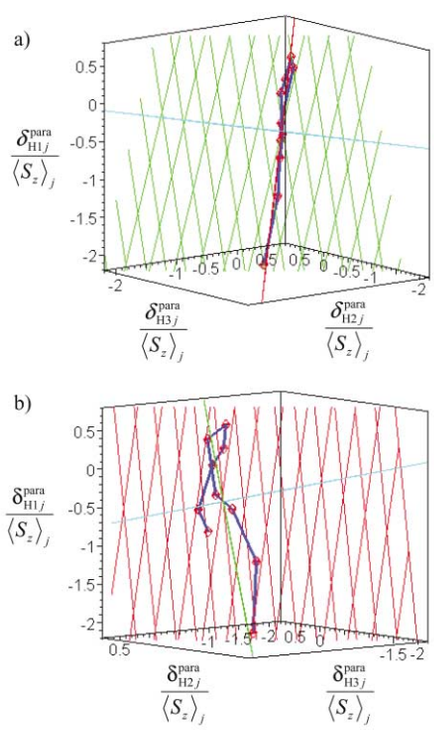

Fig. 6 3D plots of $\frac{\delta_{ij}^{para}}{\langle S_z \rangle_j}$ *vs.* $\frac{\delta_{kj}^{para}}{\langle S_z \rangle_j}$ and $\frac{\delta_{lj}^{para}}{\langle S_z \rangle_j}$ for H1, H2, H3. a) View of the best plane from profile showing the planar arrangement of the points (rhombs are used to highlight a plane orthogonal to the best plane). b) View perpendicular to the best plane showing the location of the points within the plane (the lowest point is for Ln = Ce, the highest for Ln = Dy and the last point is for Ln = Yb, the line is only a guide for the eyes and rhombs are used to highlight the best plane).

Since the three variables $\frac{\delta_{ij}^{para}}{\langle S_z \rangle_j}$, $\frac{\delta_{kj}^{para}}{\langle S_z \rangle_j}$ and $\frac{\delta_{lj}^{para}}{\langle S_z \rangle_j}$ form a homogeneous 3D cartesian *x*, *y*, *z* frame, multi-linear least-square fits of $\frac{\delta_{ij}^{para}}{\langle S_z \rangle_j}$ *vs.* $\frac{\delta_{kj}^{para}}{\langle S_z \rangle_j}$ and $\frac{\delta_{lj}^{para}}{\langle S_z \rangle_j}$ which minimize the errors along a single direction are inadequate[31] and the best least-squares planes are obtained by minimising *M* where *M* is the sum along the lanthanide series ($j = 1$ to 10 corresponding to Ln = Ce, Pr, Nd, Eu, Tb, Dy, Ho, Er, Tm, Yb) of the square of the orthogonal distances to the plane.[32] As a plane is defined by its distance to the origin and by its unit normal, $\vec{n}$, we add to *M* the constrain that $\varphi = (\vec{n} \bullet \vec{n}) - 1 = 0$ multiplied by a so called Lagrangian multiplier λ.[33] After equating all the derivatives to zero, a system of equations is found which can be solved by using software for symbolic computation,[34] thus leading to the best least-squares plane. Another possibility is to use a similar subroutine included in X-ray packages, and originally used for calculating least-squares planes passing through a fixed number of atoms which are replaced by the points $\frac{\delta_{ij}^{para}}{\langle S_z \rangle_j}$, $\frac{\delta_{kj}^{para}}{\langle S_z \rangle_j}$, $\frac{\delta_{lj}^{para}}{\langle S_z \rangle_j}$ ($j = 1$–10) defined in a cartesian *x*, *y*, *z* frame. The coefficients *a*, *b*, *c* and *d* of the resulting equation of the least-square planes

$$a\frac{\delta_{ij}^{para}}{\langle S_z \rangle_j} + b\frac{\delta_{kj}^{para}}{\langle S_z \rangle_j} + c\frac{\delta_{lj}^{para}}{\langle S_z \rangle_j} = d$$

allow the calculation of the structural factors by comparison with eqn. (12): $B_{ikl} = d/a$, $C_{ikl} = -b/a$ and $D_{ikl} = -c/a$ (Table S1, ESI). Consequently, minor uncertainties on *a* for H*ikl* triplets in which $a << b$, *c* (*i.e.* the plane is almost parallel to the *x* direction) dramatically affect the B_{ikl}, C_{ikl} and D_{ikl} parameters and these data are not used for structural comparison in the next section (see for instance H1,4,8 or H1,7,11 in Table S1, ESI). Quantitative comparisons of the experimental data $\frac{\delta_{\alpha j}^{para\ obs}}{\langle S_z \rangle_j}$ ($\alpha = i, k, l$) with those calculated in the best plane defined by eqn. (12) $\frac{\delta_{\alpha j}^{para\ calc}}{\langle S_z \rangle_j}$ ($\alpha = i, k, l$) are given by three Wilcott agreement factors[25] for each specific H*ikl* triplet along the lanthanide series:

$$AF_\alpha = \sqrt{\frac{\sum_j \left(\delta_{\alpha j}^{para\ obs}/\langle S_z \rangle_j - \delta_{\alpha j}^{para\ calc}/\langle S_z \rangle_j\right)^2}{\sum_j \left(\delta_{\alpha j}^{para\ obs}/\langle S_z \rangle_j\right)^2}}$$

where $\alpha = i, k, l$ (Table S2, ESI). These factors can be combined to give a single 'average' agreement factor characterizing each H*ikl* triplet along the lanthanide series

$$AF_{ikl} = 1/3\sqrt{AF_i^2 + AF_k^2 + AF_l^2} = \frac{1}{3}\sqrt{\frac{\sum_j \left\| a^{obs} - a^{calc} \right\|^2}{\sum_{ikl} \left\| a^{obs} \right\|^2}}$$

in which $||a^{obs} - a^{calc}||$ is the distance separating the experimental points:

$$a^{obs} = \left(\frac{\delta_{ij}^{para\ obs}}{\langle S_z \rangle_j}, \frac{\delta_{kj}^{para\ obs}}{\langle S_z \rangle_j}, \frac{\delta_{lj}^{para\ obs}}{\langle S_z \rangle_j}\right)$$

from the related calculated points a^{exp} in the best plane. The AF_{ikl} are randomly distributed around their average $\overline{AF}_{ikl} = 0.05(3)$ calculated for the 165 triplets (Table S2, Fig. S2, ESI), and their values $0.02 < AF_{ikl} < 0.17$ are similar to those found when related calculations are applied to the one-nucleus method (AF_i in Table 2). We thus conclude that $[Ln_3(L1)_3]^{9+}$

adopt a single and rigid D_3-symmetrical in solution along the complete lanthanide series in solution.

Comparison of the solution structure of $[Ln_3(L1)_3]^{9+}$ with structural models

For monometallic complexes in solution possessing at least a threefold axis, the structural parameters G_l/G_k obtained with the two-nuclei crystal-field independent eqn. (9) are ideally suited for comparing solution structures with structural models for which the geometrical terms $G_i = (3\cos^2\theta_i - 1)/r_i^3$ can be easily calculated (the threefold or fourfold axis coincides with the principal z magnetic axis).[11,15,19,35] For the D_3-symmetrical homotrimetallic complexes $[Ln_3(L1)_3]^{9+}$, we have first used the crystal structure of $[Eu_3(L1)_3](CF_3SO_3)_9(CH_3CN)_9(H_2O)_2$ [16] as a structural model for calculating θ_i^m and r_i^m (m = 1–3) according to Fig. 2 with the pseudo-C_3 axis defined as the least-square line passing through the three Eu atoms. The associated geometrical terms G_i^m (m = 1–3) are then averaged according to pseudo-D_3 symmetry to give the final set reported in Table 3. In this context we notice that the individual G_i^m terms are significantly dispersed around their D_3-average values which implies that the molecular structure of $[Eu_3(L1)_3]^{9+}$ observed in the solid state is significantly distorted from idealized D_3-symmetry.[16] The structural parameters C_{ikl}^{solid} and D_{ikl}^{solid} are then calculated with eqns. (14) and (15) and collected in Table S1 (ESI). Since the uncertainties affecting the D_3-symmetrical G_i^m values are large (*i.e.* the crystal structure deviates from D_3 symmetry), H*ikl* triplets producing $G_k^1R_{ik} - G_l^1R_{il}$ denominators close to zero give poorly reliable C_{ikl}^{solid} and D_{ikl}^{solid} parameters which cannot be used for structural comparisons (see for instance H1, 2, 3 and H2, 4, 7 in Table S1, ESI). The correlations between C_{ikl}^{solid} and $C_{ikl}^{solution}$ (Fig. 7a) and D_{ikl}^{solid} and $D_{ikl}^{solution}$ (Fig. 7b) for the 125 contributing triplets are rather poor as confirmed by the agreement factors

$$AF_{C_{ikl}} = \sqrt{\frac{\sum_{ikl}\left(C_{ikl}^{solid} - C_{ikl}^{solution}\right)^2}{\sum_{ikl}\left(C_{ikl}^{solution}\right)^2}} = 0.90 \text{ and } AF_{D_{ikl}} = 0.92$$

This strongly suggests that the solid state structure of $[Eu_3(L1)_3]^{9+}$ is not an accurate structural model for the solution structure of the D_3-symmetrical helicates, although the detailed analyses of the diamagnetic anisotropies in $[Ln_3(L1)_3]^{9+}$ (Ln = La, Y, Lu) point to very similar arrangements of the strands between the solid-state and the solution structure, as previously observed for other rigid triple-stranded helicates.[11,15,20]

An alternative explanation considers the extreme sensitivity of the C_{ikl} and D_{ikl} parameters to the exact position of the nucleus i because three paramagnetic centres contribute to the pseudo-contact shift (δ_{ij}^{pc}) as previously reported (and theoretically rationalized) in related D_3-symmetrical bimetallic lanthanide helicates.[15] Moreover, fast oscillations of the aromatic rings around their equilibrium position in solution dramatically affect G_i which have no counterpart in the solid-state.[19] In order to substantiate these hypotheses, eqns. (14) and (15) have been combined to give eqns. (22) and (23) which allow the calculation of the geometrical terms $G_l^{1solution}$ and $G_l^{2solution} + G_l^{3solution}$ for any nucleus l in solution if the geometrical terms G_i^m and G_k^m (m = 1–3) of two reference nuclei i and k are fixed.[36]

$$G_l^1 = \frac{G_i^1 - C_{ikl}G_k^1}{D_{ikl}} \quad (22)$$

$$G_l^2 + G_l^3 = \frac{\left(G_i^2 - G_i^3\right)\left(R_{ik} - C_{ikl}\right)}{R_{ik} - D_{ikl}} \quad (23)$$

Selecting H3 and H10 as references from the crystal structure of $[Eu_3(L1)_3]^{9+}$ (these protons exhibit an approximate D_3 symmetry in the solid state), the geometrical terms $G_l^{1solution}$ and $G_l^{2solution} + G_l^{3solution}$ (l = 1, 2, 4, 5, 6, 7, 8, 9, 11, Table 3) have been estimated by using the experimental structural parameters $C_{ikl}^{solution}$ and $D_{ikl}^{solution}$ found in solution (Table S1, ESI). Although the correlations between G_l^{1solid} and $G_l^{1solution}$ (Fig. 8a), and $G_l^{2solid} + G_l^{3solid}$ and $G_l^{2solution} + G_l^{3solution}$ (Fig. 8b) are approximate, the general trend is restored which indicates that the C_{ikl} and D_{ikl} parameters are highly sensitive to minor structural variations.

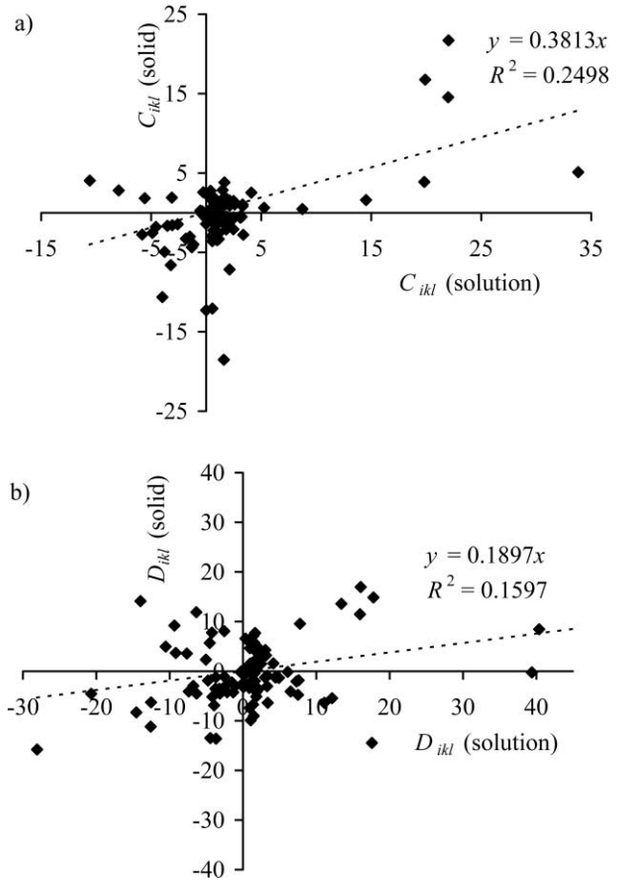

Fig. 7 Plots of a) C_{ikl}^{solid} *vs.* $C_{ikl}^{solution}$, and b) D_{ikl}^{solid} *vs.* $D_{ikl}^{solution}$ for the 125 contributing H*ikl* triplets in $[Ln_3(L1)_3]^{9+}$.

Finally, we have designed an alternative structural model by using molecular mechanics with the Amber force field in the gas phase [37] and the parameters of Durand *et al.* for the europium atoms.[38] The crystal structure of $[Eu_3(L1)_3]^{9+}$ is used as a starting model, the three Eu atom are fixed at a distance of 9.068 Å, and optimization in the gas phase (restricted to the D_3 point group) gives a second structural model with a new set of $C_{ikl}^{gas\text{-}phase}$ and $D_{ikl}^{gas\text{-}phase}$ (Table S1, ESI). Although the solid-state structure and the gas-phase model are similar (Fig. 9), the structural and geometrical parameters are completely different and only poor correlations between $C_{ikl}^{gas\text{-}phase}$ and C_{ikl}^{solid} (Fig. 10a) and $D_{ikl}^{gas\text{-}phase}$ and D_{ikl}^{solid} (Fig. 10b) are obtained for the 125 contributing triplets. This eventually confirms that the structural parameters C_{ikl} and D_{ikl} are extremely sensitive to minor structural changes and should be used with caution when comparing structural models with the solution structure. The associated correlations between $C_{ikl}^{gas\text{-}phase}$ and $C_{ikl}^{solution}$ ($AF_{C_{ikl}}$ = 0.96, Fig. S3a, ESI) and $D_{ikl}^{gas\text{-}phase}$ and $D_{ikl}^{solution}$ ($AF_{D_{ikl}}$ = 1.18, Fig. S3b, ESI) for the 125 contributing triplets are slightly worse than those obtained with the crystal structure, but the $G_l^{1solution}$ and $G_l^{2solution} + G_l^{3solution}$ (l =1, 2, 4, 5, 6, 7, 8, 9, 11, Table S2, ESI) estimated with eqns. (22) and (23) and H3 and H10 as references are similar to those obtained from the crystal structure (Fig. S4, ESI).

We conclude that (i) the triple-stranded helical structure found for $[Eu_3(L1)_3]^{9+}$ in the solid state is essentially maintained in solution except for the observation of an average D_3-

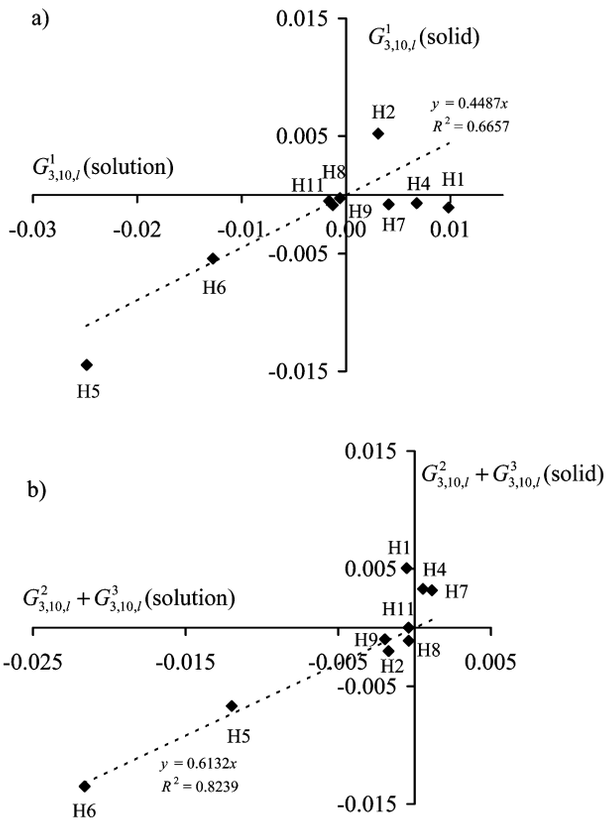

Fig. 8 Plots of a) $G_l^{1\text{solid}}$ *vs.* $G_l^{1\text{solution}}$, and b) $G_l^{2\text{solid}} + G_l^{3\text{solid}}$ *vs.* $G_l^{2\text{solution}} + G_l^{3\text{solution}}$ for H1, H2, H4, H5, H6, H7, H8, H9, H11 (H3 and H10 are taken as references, see text).

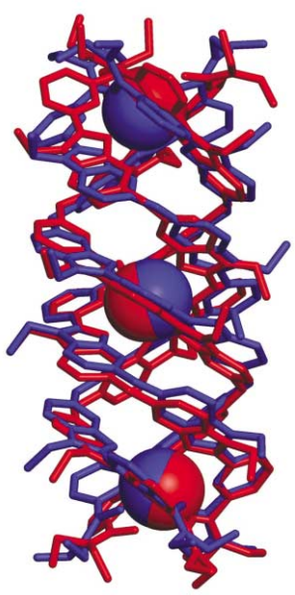

Fig. 9 Superposition of the crystal structure (in red) and the gas-phase optimized structure (in blue) of $[Eu_3(L1)_3]^{9+}$.

symmetry for the complexes $[Ln_3(L1)_3]^{9+}$ resulting from the removal of the crystal packing and (ii) the structural parameters C_{ikl} and D_{ikl} are too sensitive to minor structural changes in order to be used as reliable tests for structural comparisons. Finally, the use of the geometrical parameters obtained for the gas-phase model for performing a multi-linear least-squares fit of S_i *vs.* $G_i^{1\text{gas-phase}}$ and $G_i^{2\text{gas-phase}} + G_i^{3\text{gas-phase}}$ for the eleven aromatic protons H1–H11 in $[Ln_3(L1)_3]^{9+}$ gives $B_0^{2\text{central}} = -41(6)$ and $B_0^{2\text{terminal}} = -74(7)$ (Ln = Ce–Tb) and $B_0^{2\text{central}} = -30(7)$ and $B_0^{2\text{terminal}} = -68(8)$ (Ln = Dy–Yb) which are in good agreement with those obtained when the crystal structure is used as a structural model.

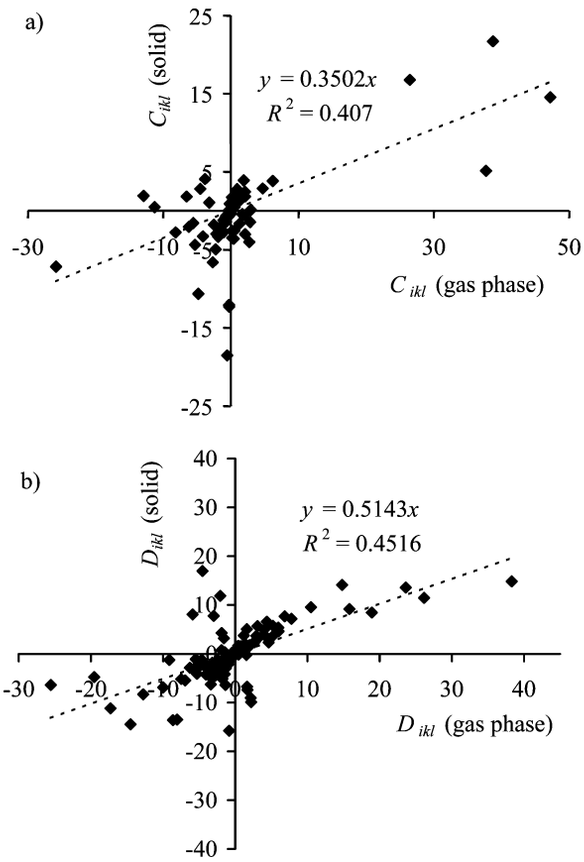

Fig. 10 Plots of a) C_{ikl}^{solid} *vs.* $C_{ikl}^{\text{gas-phase}}$, and b) D_{ikl}^{solid} *vs.* $D_{ikl}^{\text{gas-phase}}$ for the 125 contributing H*ikl* triplets in $[Eu_3(L1)_3]^{9+}$.

Conclusion

The successful derivation and application of the novel three-nuclei crystal-field independent eqn. (12) for the homotrimetallic lanthanide helicates $[Ln_3(L1)_3]^{9+}$ demonstrates that the solution structure of C_3- or C_4-symmetrical systems possessing two different metallic sites (*i.e.* two different second-rank crystal-field parameters B_0^2 according to Bleaney's approach) can be investigated by model-free methods in paramagnetic NMR. As expected from previous studies with bimetallic d–f[21,23] and f–f[15] helicates, the triple-helical wrapping of the strands produce stable and rigid $[Ln_3(L1)_3]^{9+}$ complexes in solution, whose structure is similar to that found in the solid state (X-ray diffraction), but the structural parameters C_{ikl} and D_{ikl} involved in eqn. (12) are extremely sensitive to minor structural changes because three paramagnetic centres contribute to the pseudo-contact shifts. Since deviations from the planes defined by the experimental $\frac{\delta_{ij}^{\text{para}}}{\langle S_z \rangle_j}$, $\frac{\delta_{kj}^{\text{para}}}{\langle S_z \rangle_j}$, $\frac{\delta_{lj}^{\text{para}}}{\langle S_z \rangle_j}$ points can be safely assigned to structural changes, the observation of strict planar arrangement along the complete lanthanide series (Ln = Ce–Yb) implies isostructurality for $[Ln_3(L1)_3]^{9+}$ in acetonitrile. Based on the latter result, the use of the classical one-nucleus crystal-field dependent eqn. (11) shows that the apparent 'gadolinium break' effect occurring near the middle of the series is associated with a concomitant abrupt decrease of both crystal field parameters ($B_0^{2\text{central}}$ and $B_0^{2\text{terminal}}$). At first sight, such break within an isostructural series could be traced back to the failure of Bleaney's approach for modeling magnetic anisotropies, and higher order T^{-n} ($n \geq 3$) terms should be considered[39] for complexes possessing large crystal-field splittings which do not satisfy the high-temperature hypothesis ($kT > \Delta E_{\text{CF}}$).[6,11,12] However, (i) the arrangement of the triplets $\frac{\delta_{ij}^{\text{para}}}{\langle S_z \rangle_j}$, $\frac{\delta_{kj}^{\text{para}}}{\langle S_z \rangle_j}$, $\frac{\delta_{lj}^{\text{para}}}{\langle S_z \rangle_j}$

within a single plane predicted by eqn. (12) (derived from eqn. (11)) for an isostructural series and (ii) the good correlations recently reported between Bleaney's C_j factors and the experimental anisotropic part of the magnetic susceptibility tensor for axial ($\chi^j_{zz} - \frac{1}{3}Tr\chi^j$)[11,23] and rhombic ($\chi^j_{xx} - \chi^j_{yy}$)[40,41] monometallic lanthanide complexes strongly support the view that Bleaney's approach (*i.e.* a series limited to T^{-2}) is a satisfying approximation with nitrogen and/or oxygen donor ligands. The present results thus suggest that the second-rank crystal-field parameters undergo the expected smooth decrease along the lanthanide series because of the contraction of the 4f orbitals.[5,28,29] However, this trend is amplified by the abrupt increase of the C_j parameter occurring between $4f^{1-6}$ and $4f^{8-13}$,[12] which provides an apparent abrupt break of the crystal-field parameter near the middle of the series. Finally it is worth noting that only few 'rhombic' lanthanide complexes (*i.e.* without a C_3 or a C_4 axis) have been investigated by model-free paramagnetic NMR methods[42] because eqn. (4) contains two different crystal-field parameters which prevent the use of the classical crystal-field independent eqn. (9) for testing isostructurality.[14] Since the mathematical form of δ^{pc}_{ij} given in eqn. (4) is identical to that found in eqn. (11) which holds for the homotrimetallic helicates $[Ln_3(L1)_3]^{9+}$, the novel three-nuclei crystal-field independent eqn. (12) is suitable for investigating isostructurality in rhombic systems according to Bleaney's approach if $B_0^{2\text{terminal}}(G_i^2 + G_i^3)$ is replaced with $\sqrt{6}B_2^2H_i$.

Experimental

Preparation of L1 and $[Ln_3(L1)_3](CF_3SO_3)_9$ (Ln = La, Ce, Pr, Nd, Sm, Eu, Gd, Tb, Dy, Ho, Er, Tm, Yb, Lu, Y)

The ligand 2,6-bis{1-ethyl-5-{1-ethyl-2-[6-(*N*,*N*-diethylcarbamoyl)pyridin-2-yl]benzimidazol-5-methylene}benzimidazole-2-yl}pyridine (L1) and the complexes $[Ln_3(L1)_3](CF_3SO_3)_9 \cdot xH_2O$ (Ln = La, $x = 4$; Ln = Eu, $x = 4$; Ln = Gd, $x = 2$; Ln = Tb, $x = 12$; Ln = Lu, $x = 6$) were prepared according to the literature procedure.[16] The triflate salts $Ln(CF_3SO_3)_3 \cdot xH_2O$ (Ln = La–Lu, Y) were prepared from the corresponding oxides (Rhodia, 99.99%).[43] The complexes $[Ln_3(L1)_3](CF_3SO_3)_9$ (Ln = Ce, Pr, Nd, Sm, Dy, Ho, Er, Tm, Yb, Lu) were prepared *in situ* for ^{1}H NMR studies. A solution of $Ln(CF_3SO_3)_3 \cdot xH_2O$ ($9.48.10^{-6}$ mol) in acetonitrile (1 cm^3) was added to a solution of L1 (10 mg, 9.48×10^{-6} mol) in 1 : 2 CH_2Cl_2–MeCN (1.5 cm^3). After stirring for 3 h at room temperature, the solution was evaporated, dried under vacuum and the solid residue dissolved in CD_3CN (0.7 cm^3).

Spectroscopic measurements

^{1}H NMR spectra were recorded at 25 °C on a Broadband Varian Gemini 300 spectrometer. Chemical shifts are given in ppm *vs*. TMS. The determination of longitudinal relaxation times (T_1) used the inversion-recovery technique.

Acknowledgements

This work is supported through grants from the Swiss National Science Foundation. We thank Dr G. Bernadinelli and Dr H. Flack for fruitful discussions.

References and notes

1 (*a*) D. Parker, R. S. Dickins, H. Puschmann, C. Crossland and J. A. K. Howard, *Chem. Rev.*, 2002, **102**, 1977; (*b*) J.-C. G. Bünzli and C. Piguet, *Chem. Rev.*, 2002, **102**, 1897.
2 (*a*) V. W.-W. Yam and K. K.-W. Lo, *Coord. Chem. Rev.*, 1999, **184**, 157; (*b*) I. Hemmilä, T. Ståhlberg and P. Mottram, *Bioanalytical Applications of Labelling Technologies*, Wallac Oy, Turku, 1995.
3 G. Mathis, in *Rare Earths*, eds. R. Saez Puche and P. Caro, Editorial Complutense S. A., Madrid, 1998, pp. 285–298.
4 (*a*) P. Caravan, J. J. Ellison, T. J. McMurry and R. B. Lauffer, *Chem. Rev.*, 1999, **99**, 2293; (*b*) *The Chemistry of Contrast Agents in Medical Magnetic Resonance Imaging*, eds. A. E. Merbach and E. Toth, Wiley, New York, 2001.
5 (*a*) W. T. Carnall, in *Handbook on the Physics and Chemistry of Rare Earths*, eds. K. A. Gschneidner and L. Eyring, North-Holland Publishing Company, Amsterdam, 1979, pp. 171–208; (*b*) C. Görrler-Walrand and K. Binnemans, in *Handbook on the Physics and Chemistry of Rare Earths*, eds. K. A. Gschneidner and L. Eyring, North-Holland Publishing Company, Amsterdam, 1996, vol. 23, pp. 121–283; (*c*) P. Porcher, in *Rare Earths*, eds. R. Saez Puche and P. Caro, Editorial Complutense S. A., Madrid, 1998; pp. 43–66.
6 (*a*) V. S. Mironov, Y. G. Galyametdinov, A. Ceulemans, C. Görller-Walrand and K. Binnemans, *Chem. Phys. Lett.*, 2001, **345**, 132; (*b*) V. S. Mironov, Y. G. Galyametdinov, A. Ceulemans, C. Görller-Walrand and K. Binnemans, *J. Chem. Phys.*, 2002, **116**, 4673.
7 (*a*) M. D. Kemple, B. D. Ray, K. B. Lipkowitz, F. G. Prendergast and B. D. N. Rao, *J. Am. Chem. Soc.*, 1988, **110**, 8275; (*b*) I. Bertini, C. Luchinat and G. Parigi, *Prog. Nucl. Magn. Reson. Spectrosc.*, 2002, **40**, 249.
8 (*a*) C. C. Hinckley, *J. Am. Chem. Soc.*, 1969, **91**, 5160; (*b*) J. M. Briggs, G. P. Moss, E. W. Randall and K. D. Sales, *Chem. Commun.*, 1972, 1180; (*c*) W. deW. Horrocks Jr. and J. P. Sipe, *Science*, 1972, **177**, 994; (*d*) G. E. Hawkes, D. Leibfritz, D. W. Roberts and J. D. Roberts, *J. Am. Chem. Soc.*, 1973, **95**, 1659; (*e*) W. deW. Horrocks Jr., *J. Am. Chem. Soc.*, 1974, **96**, 3022.
9 (*a*) S. Zhang, L. Michaudet, S. Burgess and A. D. Sherry, *Angew. Chem., Int. Ed.*, 2002, **41**, 1919; (*b*) S. Aime, D. D. Castelli, F. Fedeli and E. Terreno, *J. Am. Chem. Soc.*, 2002, **124**, 9364.
10 (*a*) J. H. Forsberg, in *Handbook on the Physics and Chemistry of Rare Earths*, eds. K. A. Gschneidner and L. Eyring, North-Holland Publishing Company, Amsterdam, 1996, vol. 23, pp. 1–68; (*b*) J. A. Peters, J. Huskens and D. J. Raber, *Prog. Nucl. Magn. Reson. Spectrosc.*, 1996, **28**, 283.
11 C. Piguet and C. F. C. G. Geraldes, in *Handbook on the Physics and Chemistry of Rare Earths*, eds. K. A. Gschneidner and L. Eyring, North-Holland Publishing Company, Amsterdam, 2003, vol. 33, in press.
12 (*a*) B. Bleaney, *J. Magn. Reson.*, 1972, **8**, 91; (*b*) B. Bleaney, C. M. Dobson, B. A. Levine, R. B. Martin, R. J. P. Williams and A. V. Xavier, *Chem. Commun.*, 1972, 791.
13 (*a*) C. N. Reilley, B. W. Good and J. F. Desreux, *Anal. Chem.*, 1975, **47**, 2110; (*b*) A. D. Sherry and C. F. G. C. Geraldes, in *Lanthanide Probes in Life, Chemical and Earth Sciences*, eds. J.-C. G. Bünzli and G. R. Choppin, Elsevier, Amsterdam, 1989, ch. 4.
14 (*a*) S. Spiliadis and A. A. Pinkerton, *J. Chem. Soc., Dalton Trans.*, 1982, 1815; (*b*) J. Reuben, *J. Magn. Reson.*, 1982, **50**, 233; J. Ren and A. D. Sherry, *J. Magn. Reson.*, 1996, **B111**, 178; (*c*) C. Platas, F. Avecilla, A. de Blas, C. F. G. C. Geraldes, T. Rodriguez-Blas, H. Adams and J. Mahia, *Inorg. Chem.*, 1999, **38**, 3190; (*d*) C. F. G. C. Geraldes, S. Zhang, C. Platas, T. Rodriguez-Blas, A. de Blas and A. D. Sherry, *J. Alloys Compds.*, 2001, **323–324**, 824.
15 (*a*) M. Elhabiri, R. Scopelliti, J.-C. G. Bünzli and C. Piguet, *J. Am. Chem. Soc.*, 1999, **121**, 10747; (*b*) S. Rigault, C. Piguet and J.-C. G. Bünzli, *J. Chem. Soc., Dalton Trans.*, 2000, 2045.
16 (*a*) B. Bocquet, G. Bernardinelli, N. Ouali, S. Floquet, F. Renaud, G. Hopfgartner and C. Piguet, *Chem. Commun.*, 2002, 930; (*b*) S. Floquet, N. Ouali, B. Bocquet, G. Bernardinelli, D. Imbert, J.-C. G. Bünzli, G. Hopfgartner and C. Piguet, *Chem. Eur. J.*, 2003, in press.
17 R. M. Golding and M. P. Halton, *Aust. J. Chem.*, 1972, **25**, 2577.
18 (*a*) J. P. Costes, F. Dahan, A. Dupuis, S. Lagrave and J. P. Laurent, *Inorg. Chem.*, 1998, **37**, 153; (*b*) N. Ishikawa, T. Iino and Y. Kaizu, *J. Am. Chem. Soc.*, 2002, **124**, 11440.
19 N. Ouali, B. Bocquet, S. Rigault, P.-Y. Morgantini, J. Weber and C. Piguet, *Inorg. Chem.*, 2002, **41**, 1436.
20 C. Piguet, G. Bernardinelli and G. Hopfgartner, *Chem. Rev.*, 1997, **97**, 2005.
21 C. Piguet, J.-C. G. Bünzli, G. Bernardinelli, G. Hopfgartner, S. Petoud and O. Schaad, *J. Am. Chem. Soc.*, 1996, **118**, 6681.
22 I. Bertini, C. Luchinat and G. Parigi, *Solution NMR of Paramagnetic Molecules, Current Methods in Inorganic Chemistry*, Elsevier, Amsterdam, 2001, vol. 2, pp. 263–330.
23 S. Rigault, C. Piguet, G. Bernardinelli and G. Hopfgartner, *J. Chem. Soc., Dalton Trans.*, 2000, 4587.
24 S. Rigault and C. Piguet, *J. Am. Chem. Soc.*, 2000, **122**, 9304.
25 M. R. Wilcott, R. E. Lenkinski and R. E. Davis, *J. Am. Chem. Soc.*, 1972, **94**, 1742.
26 S. Petoud, J.-C. G. Bünzli, F. Renaud, C. Piguet, K. J. Schenk and G. Hopfgartner, *Inorg. Chem.*, 1997, **36**, 5750.

27 B_0^2 is usually expressed in cm^{-1},[5] but only relative values (formally in ppm $Å^3$) are obtained from paramagnetic NMR data because Bleaney's factors are arbitrarily scaled to $C_{Dy} = -100$ and are given without units.[12].
28 T. A. Hopkins, D. H. Metcalf and F. S. Richardson, *Inorg. Chem.*, 1998, **37**, 1401.
29 A. J. Freeman and R. E. Watson, *Phys. Rev. B*, 1962, **127**, 2058.
30 J. A. Peters, *J. Magn. Reson.*, 1986, **68**, 240.
31 J. A. Irvin and T. I. Quickenden, *J. Chem. Educ.*, 1983, **60**, 711.
32 V. Schomaker, J. Waser, R. E. Marsh and G. Bergman, *Acta Crystallogr.*, 1959, **12**, 600.
33 (*a*) M. R. Spiegel, *Advanced Calculus*, Schaum's outline series, McGraw-Hill, New York, 1974, ch. 8, pp. 164 and 171–174; (*b*) P. W. Atkins, *Physical Chemistry*, Oxford University Press, Oxford, 5th edn., 1994, pp. A35–A36.
34 Maple 8, Waterloo Maple Inc., Waterloo ON N2L 5J2, Canada, 2002 (www.maplesoft.com).
35 For a theoretical justification within Bleaney's approach, see ref. 11.
36 The same approach has been used in ref. 19 for monometallic D_3-symmetrical complexes in which the position of a single nucleus has been fixed.
37 HyperChem(TM) 5.11, Hypercube, Inc., 1115 NW 4th Street, Gainesville, Florida 32601, USA, 1999.
38 S. Durand, J.-P. Dognon, P. Guilbaud, C. Rabbe and G. Wipff, *J. Chem. Soc., Perkin Trans. 2*, 2000, 705.
39 (*a*) B. R. McGarvey, *J. Magn. Reson.*, 1979, **33**, 445; (*b*) W. deW. Horrocks Jr., *J. Magn. Reson.*, 1977, **26**, 333.
40 L. Valencia, J. Martinez, A. Macias, R. Bastida, R. A. Carvalho and C. F. G. C. Geraldes, *Inorg. Chem.*, 2002, **41**, 5300.
41 (*a*) I. Bertini, M. B. L. Janik, Y.-M. Lee, C. Luchinat and A. Rosato, *J. Am. Chem. Soc.*, 2001, **123**, 4181; (*b*) M. Allegrozzi, I. Bertini, S.-N. Choi, Y.-M. Lee and C. Luchinat, *Eur. J. Inorg. Chem.*, 2002, 2121.
42 J. Reuben and G. A. Elgavish, *J. Magn. Reson.*, 1980, **39**, 421.
43 J. F. Desreux, in *Lanthanide Probes in Life, Chemical and Earth Sciences*, eds. J.-C. G. Bünzli and G. R. Choppin, Elsevier, Amsterdam, 1989, ch. 2, p. 43.
44 C. Piguet, J.-C. G. Bünzli, G. Bernardinelli and A. F. Williams, *Inorg. Chem.*, 1993, **32**, 4139.